

A propagating ERKII switch forms zones of elevated dendritic activation correlated with plasticity

Sriram M. Ajay^{1,a)} and Upinder S. Bhalla¹

¹National Centre for Biological Sciences, Tata Institute of Fundamental Research, Bellary Road, Bangalore 560065, India

(Received 19 January 2007; accepted 2 March 2007; published online 18 April 2007)

Strong inputs to neurons trigger complex biochemical events leading to synaptic plasticity. These biochemical events occur at many spatial scales, ranging from submicron dendritic spines to signals that propagate hundreds of microns from dendrites to the nucleus. ERKII is an important signaling molecule that is involved in many aspects of plasticity, including local excitability, communication with the nucleus, and control of local protein synthesis. We observed that ERKII activation spreads long distances in apical dendrites of stimulated hippocampal CA1 pyramidal neurons. We combined experiments and models to show that this >100 μm spread was too large to be explained by biochemical reaction-diffusion effects. We show that two modes of calcium entry along the dendrite contribute to the extensive activation of ERKII. We predict the occurrence of feedback between biophysical events resulting in calcium entry, and biochemical events resulting in ERKII activation. This feedback causes a switch-like propagation of ERKII activation, coupled with enhanced electrical excitability, along the apical dendrite. We propose that this propagating switch forms zones on dendrites in which plasticity is facilitated. [DOI: 10.2976/1.2721383]

CORRESPONDENCE

Upinder Singh Bhalla: bhalla@ncbs.res.in

Space is a key attribute of synaptic plasticity, both in terms of the intracellular events and in the context of the network in which the neuron is embedded. On the intracellular scale, fine details of the spatial organization of inputs have a strong influence on synaptic plasticity. These effects include heterosynaptic associativity where input at one synapse may affect plasticity at another (Engert and Bonhoeffer, 1997; Sajikumar *et al.*, 2005), and synaptic tagging, where a weakly stimulated synapse can be modified if a nearby synapse has earlier received strong input (Frey and Morris, 1997). At the dendritic scale, local alterations in dendritic excitability has been shown to play a major role in plasticity (Frick *et al.*, 2004; Hausser *et al.*, 2000). At the neuronal circuit level, the layout and placement of synapses determines the capacity for different forms of network

function. These include single-cell computational operations arising out of regulation of dendritic action potentials (Hausser and Mel, 2003; Rudolph and Destexhe, 2003; Urakubo *et al.*, 2004), and also network properties such as attractors in associative memory circuits (Frick and Johnston, 2005; Schultz and Rolls, 1999). In this study we characterize and predict the basis of this spatial unit of plasticity at the intersection of synaptic plasticity and dendritic excitability.

The extracellular regulated kinase type II (ERKII) is one of the key players in the intracellular networks mediating synaptic plasticity (Adams and Sweatt, 2002; Thiels and Klann, 2001). It responds to multiple inputs, especially Ca^{2+} (Bading and Greenberg, 1991; Dudek and Fields, 2001) and the brain-derived neurotrophic factor (BDNF) (Ying *et al.*, 2002). It mediates plasticity effects ranging from modification of structural and scaffold proteins at the synapse (Wu *et al.*, 2001) to

^{a)}Now at Temasek Lifesciences Laboratory, 1 Research Link, NUS, Singapore 117604.

transcription regulation (Roberson *et al.*, 1999) and direct phosphorylation of ion channels critical for setting neuronal excitability (Yuan *et al.*, 2002; Zhu *et al.*, 2002). One of the important ERKII targets in neurons is the A-type potassium channel KV4.2 (Yuan *et al.*, 2002). Phosphorylation of this channel leads to its inactivation and hence lowers K⁺ efflux from the cell. The net result of this phosphorylation is therefore an increase in neuronal excitability (Morozov *et al.*, 2003).

The intracellular network involving ERKII is richly connected, and it is therefore difficult to assess all the upstream and downstream events that occur when it is activated. This becomes still more difficult in the neuronal context, where the long and narrow processes and highly dynamic inputs can lead to large activity differences between different regions of the cell and dendritic tree. Computer simulations based on biochemical reconstructions of signaling interactions offer one way to understand and predict the behavior of such systems (Bhalla *et al.*, 2002).

In this study we started with the simple observation that ERKII was activated along a surprisingly large section of dendrite following a stimulus that triggered synaptic change. We asked if this spread could be explained through reaction-diffusion biochemistry. Our experiments ruled out models that only involved biochemical spreading. We then asked whether the spread was due to diffuse synaptic input, or due to dendritic action potentials causing Ca²⁺ influx. We found that both effects contributed to the spread of ERKII activation. Finally, we broadened our analysis further and tested if feedback between electrical and biochemical signaling events could amplify the spread. We predict that there is a >100 μm extent of elevated ERKII activity in the dendrite due to this feedback, which may form a zone in which synaptic plasticity is facilitated.

RESULTS

ERKII is activated along long segments of apical dendrite

ERKII is a sensitive readout of neuronal plasticity (Ajay and Bhalla, 2004; Dudek and Fields, 2001). We used immunohistochemistry to measure the spatial extent of dendritic activation of ERKII following long-term potentiation (LTP)-inducing stimuli. We found that long segments (>100 μm) of the primary apical dendrite show *p*-ERKII staining (Fig. 1). How does this staining correlate with LTP amplitude? In earlier studies, we have shown that field recordings and Western blot studies show a strong correlation between ERKII activation and biophysical readouts of plasticity (Ajay and Bhalla, 2004). Dudek and Fields have shown that an increasing fraction of the CA1 shows ERKII staining as stimulus current is increased (Dudek and Fields, 2001). These are both averaged readouts over a large portion of the CA1. In the current experiments we utilized massed (three tetanic bursts at 100 Hz, separated by 20 s each) and spaced

(three tetanic bursts at 100 Hz, separated by 5 min each) stimuli, respectively, so as to probe how ERKII activation spread depends on stimulus characteristics. We had earlier found that spaced stimuli elicit approximately twice the LTP amplitude as massed stimuli and also approximately twice the ERKII activity as measured by Western blots (Ajay and Bhalla, 2004). Here we found that *p*-ERKII staining was discrete, and appeared to stain a subset of dendrites in an all-or-none manner (Fig. 1). Consistent with our earlier findings, spaced stimuli (higher LTP amplitude) give an approximately two-fold greater number of dendrites staining for *p*-ERKII than massed stimuli [Figs. 1(C) and 1(D) S2]. We confirmed that the *p*-ERKII staining we observed was largely in the dendrites as it colocalized with antibody staining for dendritic marker MAP-2 (Fig. 1(E)).

We also examined *p*-CaMKII as a synaptic plasticity marker. We costained slices with *p*-ERKII and *p*-CaMKII after spaced tetanic stimuli. We observed some colocalization between the two activated molecules, but also dendrites that did not co-stain (Fig. 1(F)). This was consistent with our observations in an earlier study where we found that there was little correlation between the time scales of activation of the two kinases for this stimulus pattern (Ajay and Bhalla, 2004). ERKII is also activated by damage due to slicing and electrode pressure (Supplementary Fig. S1) so we took care to subsection our slices using only the innermost 200 μm of the 400 μm slices, and to use a restricted region of CA1 for our analysis that was between the two electrodes. To show that ERKII activation in the inner layers of the slice was stimulus driven and not artifactual, we performed immunohistochemistry to compare the extent of ERKII activation in the superficial as opposed to the inner 200 μm layers of the slice. We performed a statistical analysis of ERKII activation as measured by numbers of stained dendrites. We compared the statistics for superficial layers with inner 200 μm statistics for test pulses, massed stimuli, and spaced stimuli. We show that all cases differ from each other, and differ strongly ($p < 1.75 \times 10^{-6}$) from the statistics for superficial layers (Supplementary Fig. S2). Under all experimental conditions, the superficial layer staining was much larger than the inner layers.

These initial experiments showed that ERKII activation in hippocampal CA1 neuron dendrites had two interesting properties. First, it appeared as all-or-none labeling in a distinctly labeled subset of dendrites. Increased LTP amplitude correlated with increased numbers of activated dendrites and not with staining intensity. Second, ERKII activation extended over long, >100 μm stretches of apical dendrite. This extended activation occurred for massed as well as spaced stimuli even though they resulted in very different levels of LTP and different numbers of stained dendrites. We followed up these observations with experiments and computational models to understand these two properties.

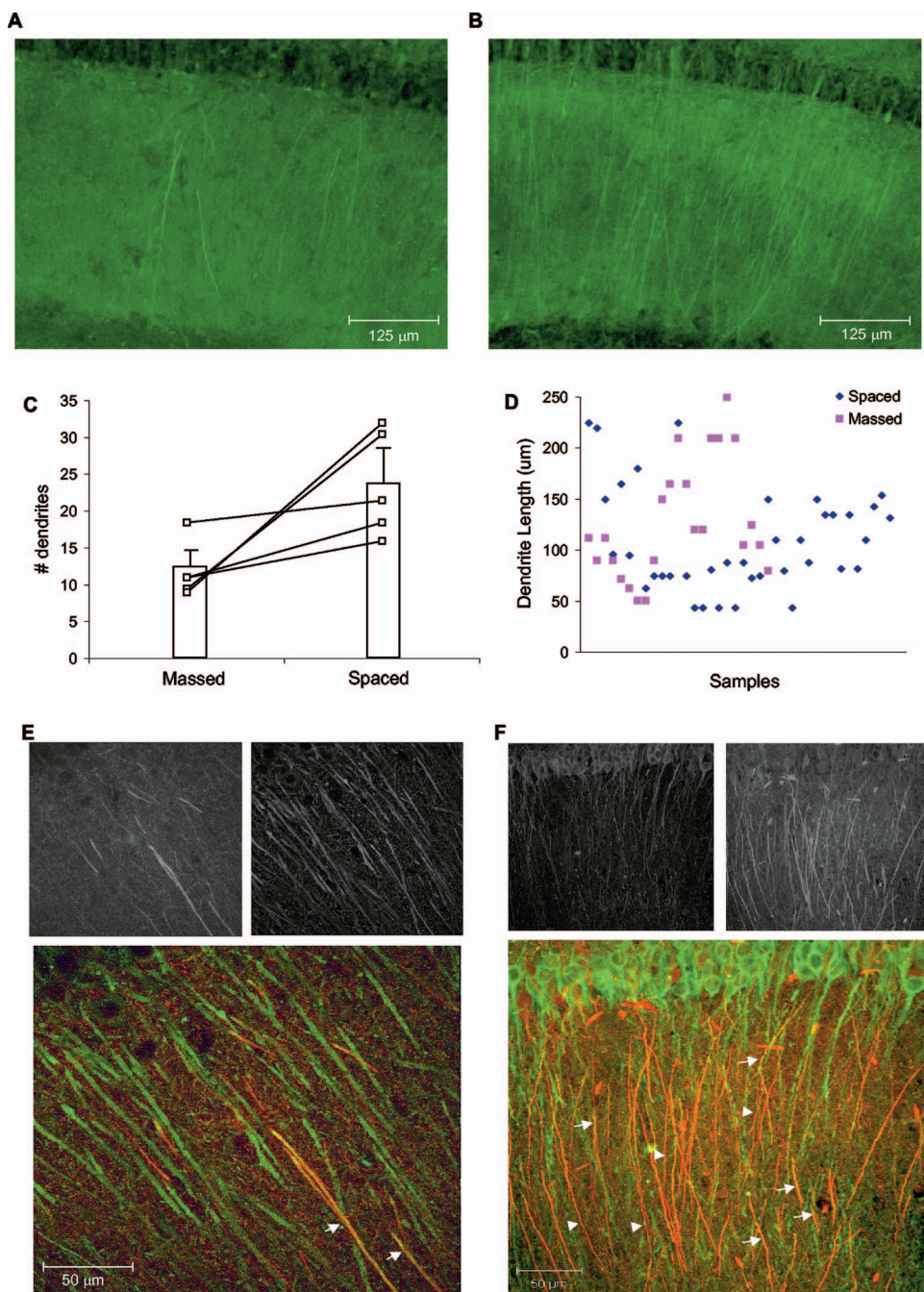


Figure 1. Extensive dendritic ERKII activation following LTP stimuli. Fluorescence images of A, and B: *p*-ERKII staining monitored 10 min after the last stimulus, for massed and spaced stimuli, respectively. In both cases long segments of dendrite are activated, but many more segments are activated for the spaced stimuli in B. Scale bar is 125 μm . C: Statistics on the number of *p*-ERKII labeled dendrites. There are significantly more labeled dendrites for the spaced stimuli ($p < 0.05$). All experiments were conducted in pairs so as to minimize differences in sample preparation (lines between data points), with one massed and one spaced stimulus set performed on slices from the same hippocampus. D: Distribution of lengths of stained dendrites. The scatter plots overlap completely. Confocal images of E: *p*-ERKII staining colocalizes with dendritic marker MAP-2. *p*-ERKII (red), MAP2 (green) in the merge. Arrows point to dendrites that show colocalization. F: *p*-CaMKII (green) and *p*-ERKII (red) show very limited overlap in the merge. Arrows point to examples of dendrites that show colocalization; arrowheads point to dendrites that have only *p*-ERK II staining.

Thresholding in ERKII activation

We developed computational models of biochemical signaling to understand the apparent all-or-none staining of *p*-ERKII in the apical dendrites. We considered the proper-

ties of a small segment (compartment) of the apical dendrite that was assumed to be spatially homogenous [Fig. 2(A)]. The compartment was 10 μm long and 4 μm in diameter. We considered two models for signaling in the compartment.

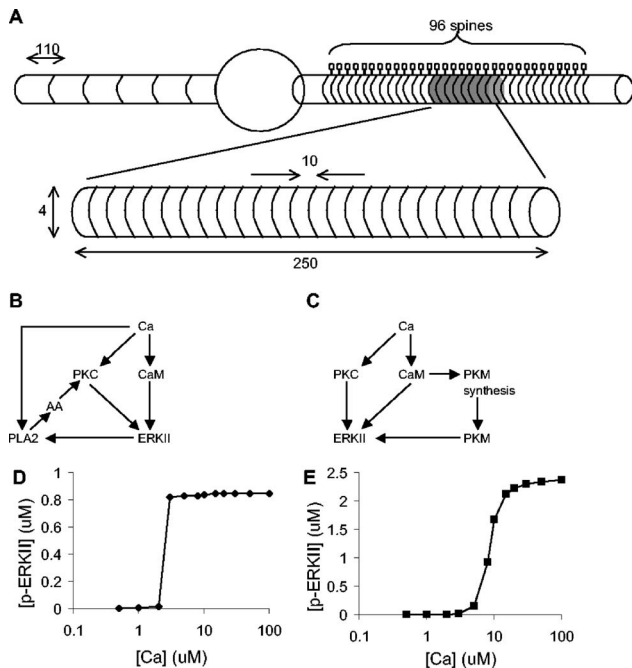


Figure 2. Biochemical reaction-diffusion model. A: Spatial structure of the model in relationship to the pyramidal neuron apical dendrite. The set of 25 diffusing compartments (shaded) are approximately in the middle of the apical dendrite. Each compartment is 10 μm in length and 4 μm in diameter. B: Bistable feedback model schematic. In this, ERKII is activated by CaM as well as PKC. ERKII phosphorylates PLA2 to raise its activity, and the resultant synthesis of AA activates PKC. PKC acts on the upstream molecules in the ERKII pathway (via Ras and Raf) to complete the feedback loop. C: Singly stable feedforward model schematic. Ca²⁺ influx triggers PKM synthesis as well as more rapid ERKII activation. PKM elevation increases ERKII activity. Due to slow turnover of PKM (model parameters) this elevation lasts for ~1 h. D: Sharp threshold for ERKII activity as a function of the Ca²⁺ input for the bistable feedback model. E: Steep threshold for ERKII activity as a function of the Ca²⁺ input for the feedforward PKM model. Both models show a threshold in the 1–10 μM Ca²⁺ range.

The first [Fig. 2(B)] incorporated a positive feedback loop: ERKII activated phospholipase A2 (PLA2), PLA2 activated protein kinase C (PKC), and PKC activated ERKII. This was a simplified version of earlier models of ERKII and neuronal signaling (Bhalla and Iyengar, 1999; Bhalla *et al.*, 2002). The biochemical properties of the earlier model were extensively tested in a fibroblast cell line (Bhalla and Iyengar, 1999; Bhalla *et al.*, 2002), so we believe that the neuronal variant of the model is at least semiquantitatively correct in its biochemical properties. This model was bistable, that is, it had memory switch-like characteristics including sharp turn on as a function of the Ca²⁺ stimulus [Fig. 2(D)]. Thus, it explained thresholding in *p*-ERKII staining in the dendrite. We refer to this model as the bistable model.

The second model was a feedforward circuit involving the activation of ERKII directly through CaM and PKC, and also involving Ca²⁺-triggered synthesis of PKM [Fig. 2(C)],

(Ajay and Bhalla, 2004; Hernandez *et al.*, 2003). The synthesized PKM also activated ERKII, leading to feedforward activation on a longer time course than brief Ca²⁺ stimuli. We refer to this model as the PKM model. This model was based on our earlier work involving the semiquantitative biochemical characterization of both ERKII and CaMKII activity in the hippocampal slice under similar experimental conditions as the current study (Ajay and Bhalla, 2004). Therefore, this model also draws upon direct biochemical information. This model also had a steep turn on as a function of the Ca²⁺ stimulus, in this case arising from the steep activation curves of CaM [Fig. 2(E)]. Thus, this model was also a partial explanation for all-or-none *p*-ERKII staining.

In addition to this form of thresholding, it is also known that antibody staining can introduce strongly nonlinear effects, which can also result in all-or-none staining (Belanger *et al.*, 1996). Thus these data, along with our initial models, may explain some of the all-or-none staining but do not address the spatial extent of ERKII activation.

Measuring ERKII activity spread

Preliminary calculations suggested that the time course of ERKII activation spread was an important test to narrow down the possible models that might be able to explain the phenomenon. We therefore performed additional experiments to measure ERKII spread at different time points after the application of the same stimuli as in the experiments above. These experiments were designed to narrow down model possibilities. We obtained staining profiles for three time points: 1, 10, and 45 min after the end of the stimulus. In all these and subsequent tests, the stimulus was three bursts of 100 Hz tetanus for 1 s each, separated by 5 min, which is spaced stimuli. Overall, we see extensive staining (>100 μm) at all three time points (Fig. 3). There was no significant difference between the staining lengths.

Five spatial models for ERKII activity spread

Here we addressed our first hypothesis: that ERKII activation spread was too broad to occur through reaction-diffusion biochemistry. We took our observations of extensive ERKII staining (Fig. 3) as a starting point. We incorporated space and diffusion into our models of dendritic ERKII signaling. We did this by replicating each of the single compartment models considered above, 25 times along the length of the dendrite, so as to model a 250 μm stretch [Fig. 2(A)]. In one case we modeled 40 compartments to monitor longer-range spreading. We included terms for the diffusive exchange of molecules between the compartments so as to obtain a reaction-diffusion model.

We considered five specific reaction-diffusion models for the spread of ERKII activation to test if they could account for our results from Fig. 3: (1) single-point Ca²⁺ influx, simple diffusion, (2) single-point Ca²⁺ influx, diffusion + active transport, (3) single-point Ca²⁺ influx, diffusion + bista-

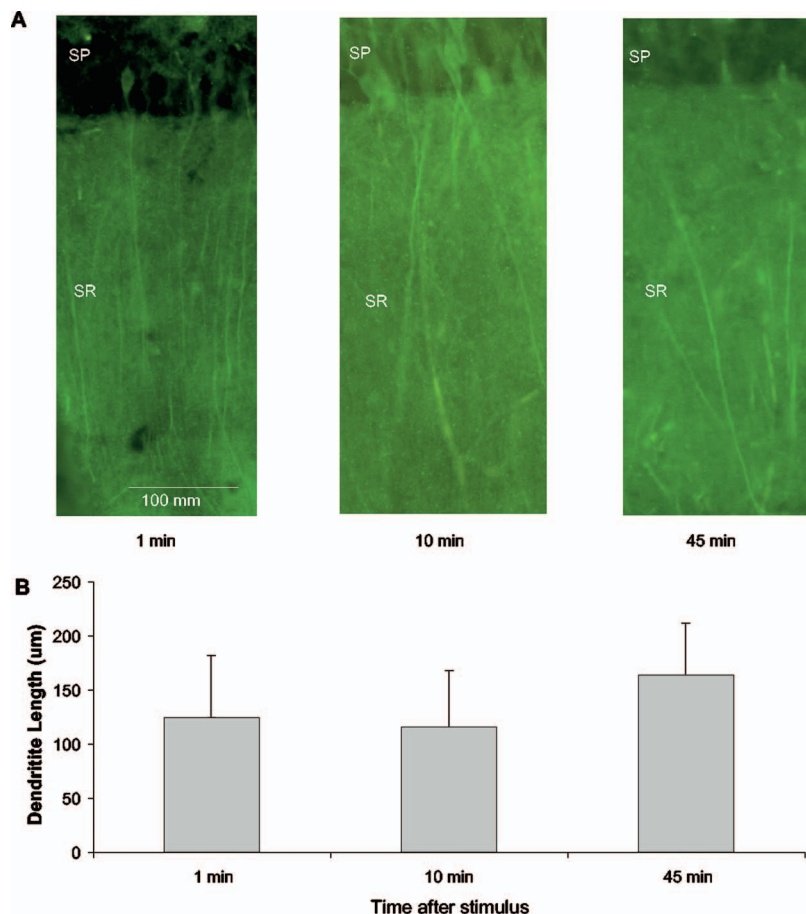


Figure 3. ERKII spread is rapid and sustained.

A: *p*-ERKII staining in dendrites sampled at 1, 10, and 45 min after the end of stimulus. In all cases long segments of dendrite are activated in a subset of cells. B: Distribution of stained lengths at different times.

bility, (4) multipoint Ca^{2+} influx + diffusion, and (5) uniform Ca^{2+} influx due to dendritic action potentials. All except model (3) utilized the feedforward, PKM synthesis model from Fig. 2(C). Model (3) used the bistable biochemical feedback circuit from Fig. 2(B). In all cases the input stimulus was a series of three square pulses of Ca^{2+} applied to one or more compartments. Except for model (2) the pulse duration was 1 s. We had two primary criteria for successful models: The *p*-ERKII levels should exceed 10 nM, to account for staining, and the extent of the staining should be at least 100 μm at all time points, as seen in the experiments. The outcomes of these simulations were as follows.

Reaction-diffusion model (1): single-point Ca^{2+} influx, simple diffusion. This model failed on two counts: narrow spatial spread and low amplitude at 45 min. (Figs. 4(A) and 4(B)). Even for moderate diffusion ($1 \mu\text{m}^2/\text{s}$), the spatial spread was too small. More rapid diffusion of $10 \mu\text{m}^2/\text{s}$ (not shown) gave still lower amplitudes of *p*-ERKII. Even for slow diffusion [$0.1 \mu\text{m}^2/\text{s}$, Fig. 4(B)] the level of *p*-ERKII at 45 min was very low (<1 nM), which is well under 1% of the peak ERKII activity.

Reaction-diffusion model (2): local Ca^{2+} influx, diffusion + active transport. In this model the transport occurs from the stimulus site toward the cell body, i.e., from left to right in the figure. As a result, activity upstream of the stimulus (to the

far left of the figure) is small, activity at the stimulus point is moderate, and there is a tail of transported *p*-ERKII toward the right. This model failed because it gives rise to extremely low ERKII activity. We modeled $1 \mu\text{m}/\text{s}$ transport rates (Kennedy and Ehlers, 2006) for all molecules. We used a longer section of dendrite in this model (40 compartments of 10 μm each) in order to monitor signal propagation down the length of the dendrite. We found that the original stimulus conditions produced very small responses, so we considerably increased our stimulus strength. We show results [Figs. 4(C) and 4(D)] for a local stimulus delivered on five compartments, at twice the amplitude, and for 5 s rather than 1 s duration. Despite this 50-fold increase in total stimulus amplitude as compared to model (1), the *p*-ERKII level was small (~ 4 nM) even at the 1 min time point, and for later times the response was vanishingly small. The low amplitude was because the transport processes caused a washout of activated molecules, so the successive stimuli did not have an opportunity to give a buildup of responses. Other variants on model (2), with transport restricted to *p*-ERKII, also had responses below 10 nM and were therefore rejected (data not shown).

Reaction-diffusion model (3): single-point Ca^{2+} influx, diffusion + bistability. This model failed because it did not reach 100 μm spread even at the 45 min time point. Bio-

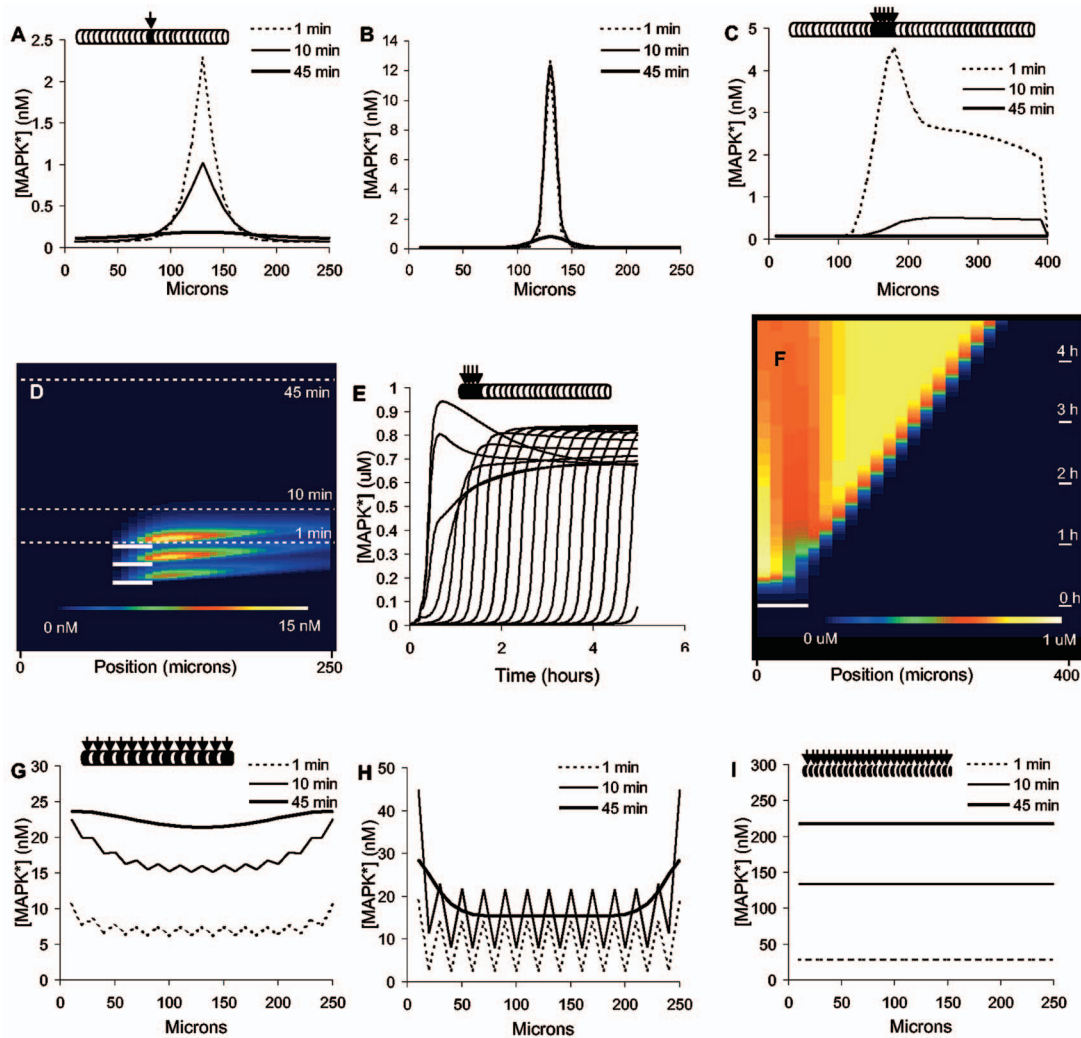


Figure 4. Five reaction-diffusion models for ERKII activation spread. In each of the left-hand panels a schematic of the 25-compartment model is provided, where the arrow and dark shading indicate stimulus point(s). A: Point stimulus with diffusion at $1 \mu\text{m}^2/\text{s}$. Spread is too narrow at 1 and 10 min, and too shallow at 45 min. B: Point stimulus with diffusion at $0.1 \mu\text{m}^2/\text{s}$. Spread is too narrow in all cases, and too shallow at 45 min. C and D: Point stimulus with diffusion at $0.1 \mu\text{m}^2/\text{s}$ plus ERKII transport at $1 \mu\text{m}/\text{s}$. This model does show spreading but the response amplitude is too small. The stimulus is twice as large, $5\times$ the width and $5\times$ the duration of that in B. There is significant spread toward the positive x axis at 1 and 10 min, but the amplitude is very small even with this 50-fold larger stimulus. At 10 and 45 min the response has declined still further. D: The same simulation with time-space color plot. The 40 compartments of the model are on the x axis, and time is on the y axis. Stimuli are delivered at five compartments at the time and location indicated by the three heavy white bars. Sampling times are indicated by dashed lines. Transepts through these lines give the plots in C. E and F: Stimulus of $20 \mu\text{M}$ Ca^{2+} into four compartments of the 25-compartment bistable model with diffusion at $0.1 \mu\text{m}^2/\text{s}$. Activity propagates through the entire dendrite, but far too slowly to account for p -ERKII staining. E: Time course of activation of successive compartments. F: Time-space color plot of the same data. A single stimulus is given on four compartments at the time and location indicated by the white bar. G: Multiple-point stimulus delivered on alternate compartments when diffusion is $1 \mu\text{m}^2/\text{s}$. This is consistent with the experimental data. Response is larger at the edge of the simulation due to boundary effects. H: Same stimulus, $D = 0.1 \mu\text{m}^2/\text{s}$. Response is spotty for 1 and 10 min responses, but is otherwise consistent with the experimental results. I: Multiple-point stimulus delivered on all compartments. Response is consistent with experiment. As expected, the responses in all compartments are the same.

chemical activity propagation is an attractive mechanism and several studies have looked at its role in signal spread (Kholodenko, 2003; Reeves *et al.*, 2006; Reynolds *et al.*, 2003). We conducted wide parameter searches to see if there were conditions under which the speed of propagation in-

creased (Supplementary Fig. S9). The fastest propagation time of $\sim 0.03 \mu\text{m}/\text{s}$ occurred when the model was held very close to activation threshold, but even this was too slow to account for our data. Furthermore, this model was very fragile, because even a small change in model conditions

could cause spontaneous activation of the feedback, or could eliminate propagation altogether. This degree of fragility argues against such a model.

Reaction-diffusion model (4): multipoint Ca^{2+} influx + diffusion. This model may work. We considered several different cases for input spacing and diffusion constant. Data shown are for input on every alternate compartment and diffusion constants of 1 and $0.1 \mu\text{m}^2/\text{s}$, respectively (Figs. 4(G) and 4(H)). Except for the edge effects for the last compartments, the ERKII activation was reasonably large and extended over the entire simulated dendrite. For slower diffusion rates the activation was somewhat spotty, and the predicted staining may be patchy depending on the resolution of the antibody method.

Reaction-diffusion model (5): uniform Ca^{2+} influx due to dendritic action potentials. This model may work. We modeled this by assuming that the action potentials caused an equal influx of calcium (for $1 \text{ s} \times 3$ stimuli) into all compartments. Not surprisingly, the outcome was that there was uniform and large activation of ERKII on all dendrites [Fig. 4(I)].

In summary, reaction-diffusion models (1)–(3) failed to match our experimental observations. We were left with two models in which stimuli arrived at many points along the dendrite, either through broad synaptic connectivity, or through dendritic action potentials. We inferred that reaction-diffusion or transport effects alone could not explain our observations of rapid, extended ERKII activation. Synaptic input and electrical properties of the neuron must therefore also be included to understand our experiments. Our next step was to devise experiments and models to take these further properties into consideration.

Electrical model of CA1 pyramidal neuron

We developed an electrical model of the hippocampal CA1 neuron to act as an interface between our experimental design with electrical stimuli, and our biochemical model with the *p*-ERKII readout. The electrical model was designed to account for cellular biophysical effects starting from details of synaptic input and resulting in spatial and temporal profiles of calcium influx into dendrites. We implemented a compartmental electrical model of the hippocampal CA1 pyramidal neuron that also included Ca^{2+} dynamics. This was a relatively simple unbranched model of the pyramidal neuron and was based on a model by Traub (Traub *et al.*, 1991) as implemented in GENESIS (Bower and Beeman, 1998). We added 96 compartments bearing dendritic spines having alpha-amino-3-hydroxy-5-methyl-4-isoxazole propionic acid (AMPA) and N-methyl-D-aspartate (NMDA) receptors. We paid particular attention to Ca^{2+} dynamics within the spine and in the dendritic compartment, including fluxes for diffusion, pumps, and voltage and ligand-gated channels [Fig. 5(C)]. We implemented decremental Na-channel levels more distal to the soma, to obtain falloff of dendritic action

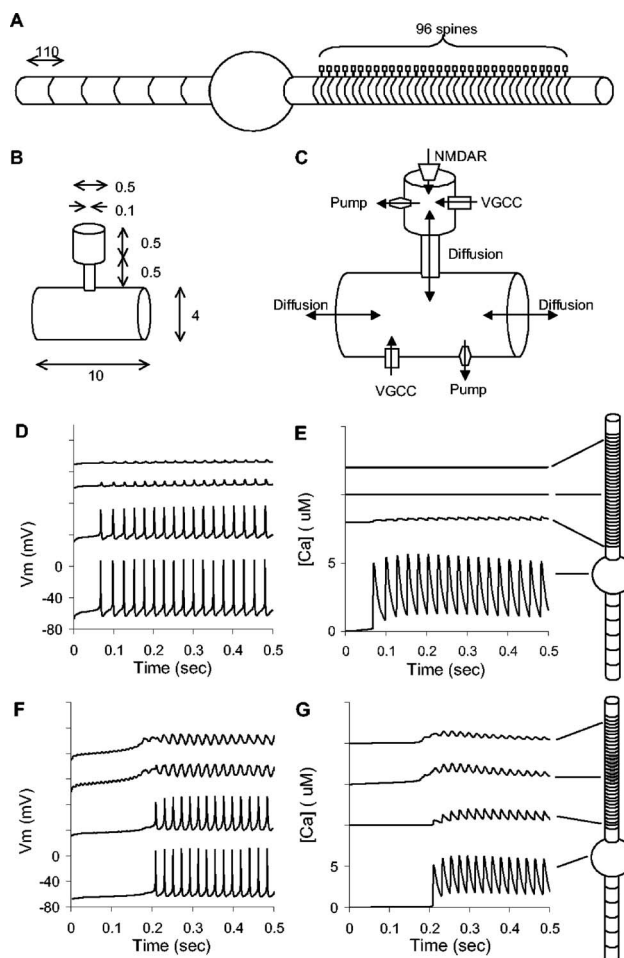


Figure 5. Electrical compartmental model. A: Basic model geometry. Basal compartments (to the left) are $110 \mu\text{m}$. B: Compartment and spine geometry in apical dendrite. C: Calcium dynamics and fluxes in the model. D and E: Cellular response to somatic depolarization. D shows membrane potential at soma and three different points on the apical dendrite. Tick marks are at 40 mV , and each trace starts at -70 mV . E shows the Ca^{2+} levels at the same points. Tick marks are $5 \mu\text{M}$, each trace starts at $0 \mu\text{M}$. F and G: Cellular response to the 100 Hz tetanic stimulus in the middle 24 compartments of apical dendrite (shaded compartments in model schematic). F: Membrane potential, tick marks at 40 mV . Note the much larger responses in the more distal regions of the dendrite, compared to panel D. G: Ca^{2+} concentration, tick marks at $5 \mu\text{M}$. Note the much larger Ca^{2+} responses in the distal dendrites, as compared to panel E.

potentials more distant from the cell body [Fig. 5(D)], (Bernard and Johnston, 2003; Frick *et al.*, 2004). Other channels may also have spatial variability in their distribution, but given the simplified dendritic structure of our model we did not incorporate this additional detail. Model details are presented in the Supplemental material S8. This model exhibited local calcium influx when stimuli were delivered in the apical dendrite [Figs. 5(F) and 5(G)]. To couple the calcium output to the biochemical model, we took the predicted calcium levels for 25 dendritic compartments in the middle of

the apical dendrite and used these as the input to the reaction-diffusion model (1) as analyzed above. Overall, this gave us a loosely coupled model incorporating both cellular biophysics and reaction-diffusion signaling chemistry (Supplementary data S8; methods). We used this loosely coupled model for the next two cycles of matching experiment to model.

Effects of local synaptic input: Experiment and model

We first tested the possibility suggested by reaction-diffusion model (4), that ERKII activation depends on local synaptic input. We carried out experiments where synaptic input was present only on a portion of the apical dendrites, and monitored how ERKII activation spread beyond the input zone. In these experiments, we cut part of the slice so as to sever a portion of the Schaffer collateral bundle. Assuming that a majority of the projections continue in parallel, this should eliminate synaptic input proximal to the cell body layer (the Stratum Pyramidale, SP). We found that this manipulation eliminated ERKII activation proximal to the SP [Figs. 6(A) and 6(B)]. We measured the distance that the cut extended past the SP, and assumed that we had severed all inputs more proximal to the soma than this length. We measured the range of propagation of staining in ERKII-active dendrites as the extent of staining past the cut position. The range of fall-off of ERKII activation was around 35 μm but with considerable scatter [Figs. 6(C) and 6(E)]. The manipulation in this experiment only removes input, without affecting local dendritic mechanisms of diffusion, bistable wave propagation, or transport as mechanisms for spatial spread. Thus, the restricted spread of ERKII activation is direct confirmation of the simulation results that rule out reaction-diffusion models (1), (2), and (3). We consider reaction-diffusion model (5) in a later section.

We now set up the model to simulate the same cut-slice manipulation, by providing synaptic input only to the distal portion of the modeled apical dendrite [Fig. 6(D)]. As described above, we fed the output of the biophysical model (the calcium concentration in the dendritic compartments) into the corresponding biochemical model. We measured the falloff of ERKII in the model as the length scale for a fall from 80% to 20% activation, and compared this with experiment [Figs. 6(D) and 6(E)]. We performed parameter exploration to find conditions where the model best matched the experimentally observed length scale of ERKII activity fall-off. We varied three major parameters: the amplitude of the Ca^{2+} input, the number of spines per compartment (which represents both synaptic strength and spacing in the model), and the diffusion constant (Supplementary Figs. 9G–9J). We obtained our best match (smallest length scales) when the Ca^{2+} peak input was 5–10 μM (a scale factor of 10–20), the number of spines was 2 or 5, and the diffusion was 0.1 $\mu\text{m}^2/\text{s}$. As this length of $\sim 60 \mu\text{m}$ is still larger than the

experimental length scale of 35 μm , we additionally assume that there is some nonlinearity in antibody staining (Belanger *et al.*, 1996).

This cut-slice experiment and model therefore show that ERKII activation requires local synaptic input, even if voltage-gated calcium channels (VGCCs) are not blocked. A weak but diffuse synaptic projection is required to sustain the extended ERKII activation, and there is about 35 μm of spreading of ERKII activation past the stimulus site.

Effects of dendritic Ca^{2+} influx: Experiment and model

We then considered the alternate possibility from reaction-diffusion model (5), which suggests that dendritic action potentials lead to extensive Ca^{2+} influx and uniform ERKII activation along large stretches of dendrite. We performed experiments to manipulate calcium influx and monitor their effects on ERKII activation spread. We blocked dendritic calcium influx through VGCCs—*L*, *R*, and *T* by applying Nifedipine and NiCl_2 in the bath (Hoogland and Saggau, 2004). These reagents should substantially block back-propagating action potentials, and strongly reduce calcium influx, and we used levels of NiCl_2 that should not affect NMDA receptor (NMDAR) conductances (Methods). We found that the extent of dendritic activation of ERKII was considerably shortened, coming down to $\sim 50 \mu\text{m}$ as against $>100 \mu\text{m}$ in the control case (Fig. 7). Notably, the staining was strong even though it was shorter in length. LTP levels were measured 45 min after the last tetanic stimulus. These levels appeared to be slightly reduced as compared to control, but this decrease was not significant. The experiment showed that VGCCs play a major role in the spread of *p*-ERKII in dendrites. As a control, we also blocked synaptic calcium entry through NMDA receptors using AP-5 and found that staining [Supplementary Fig. S1(C)] as well as LTP were eliminated, as expected (data not shown). These results are consistent with earlier studies that have also reported that VGCC block does not eliminate dendritic ERKII activation, but NMDAR block does (Dudek and Fields, 2001).

We now modeled these effects using the same loosely coupled model as in the cut-slice experiment, which combined both the electrical and biochemical models. We modeled the VGCC block experiment by setting the conductance of VGCCs in the biophysical model to zero. We then applied inputs to a single point in the biophysical model (i.e., to a 10 μm compartment), and used the model to predict calcium levels at different times and positions along the dendrite [Fig. 7(C)]. These calcium values were fed into the biochemical model, and ERKII activation simulated [Fig. 7(D)]. As before, we explored different combinations of Ca^{2+} input, the number of activated spines, and the diffusion constants [Supplementary Figs. S9(C)–9(F)]. The best fit to experimental data was obtained with the Ca^{2+} scaling factor of 10 (5 μM peak), the number of activated spines=50, and *D*

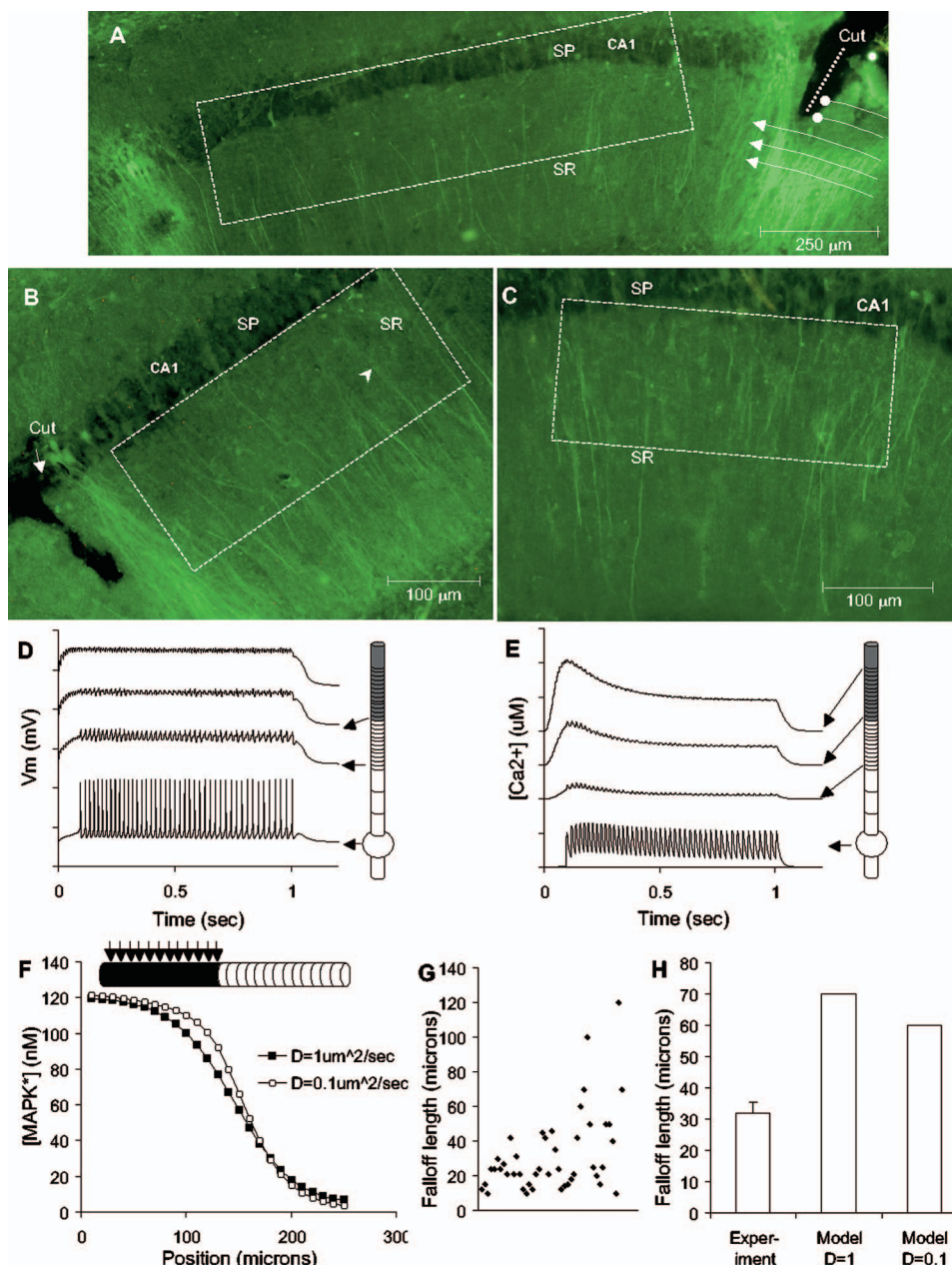


Figure 6. ERKII activation spread requires local synaptic input. A–C: *p*-ERKII labeled fluorescence images of the CA1 region. Boxed regions in A, B, and C indicate the area of analysis. Intense staining outside this area is likely to be due to injury because of the cutting or electrode pressure. A: Slice with cut in Schaffer collateral bundle, indicated by arrows to right of image. The dendritic staining for *p*-ERKII is present in most of the stratum radiatum (SR), but is truncated at the level of the cut. Scale bar 250 μm . B: Higher magnification image of a different cut slice. The arrowhead indicates the region of *p*-ERKII staining falloff. Scale bar 100 μm . C: Control slice showing *p*-ERKII staining right up to the stratum pyramidale (SP). Scale bar 100 μm . D: Electrical activity at different points along the simulated neuron, stimulated only in the shaded region. Each vertical division is 40 mV. E: Calcium levels at different points along the same simulated neuron. Each vertical division is 5 μM . F: Simulations of *p*-ERKII activation using the Ca²⁺ input from panel E. These simulations used an input density of 5 synaptic inputs per compartment. G: Scatter plot of the length of *p*-ERKII staining falloff in experiments. H: Comparison of experimental and simulated length scales of falloff. The simulated falloff length is measured as the range from 20% to 80% of the maximum.

$=0.1 \mu\text{m}^2/\text{s}$. The extent of ERKII activation was 50 μm in this case, which matched the experimental value. If inputs were given to multiple adjacent compartments in the model, the spatial extent of ERKII activation increased (data not

shown). We therefore infer that a strong, single-point stimulus is most consistent with the experimental data.

The VGCC blocking experiment and model showed that dendritic calcium influx through VGCCs was a key determi-

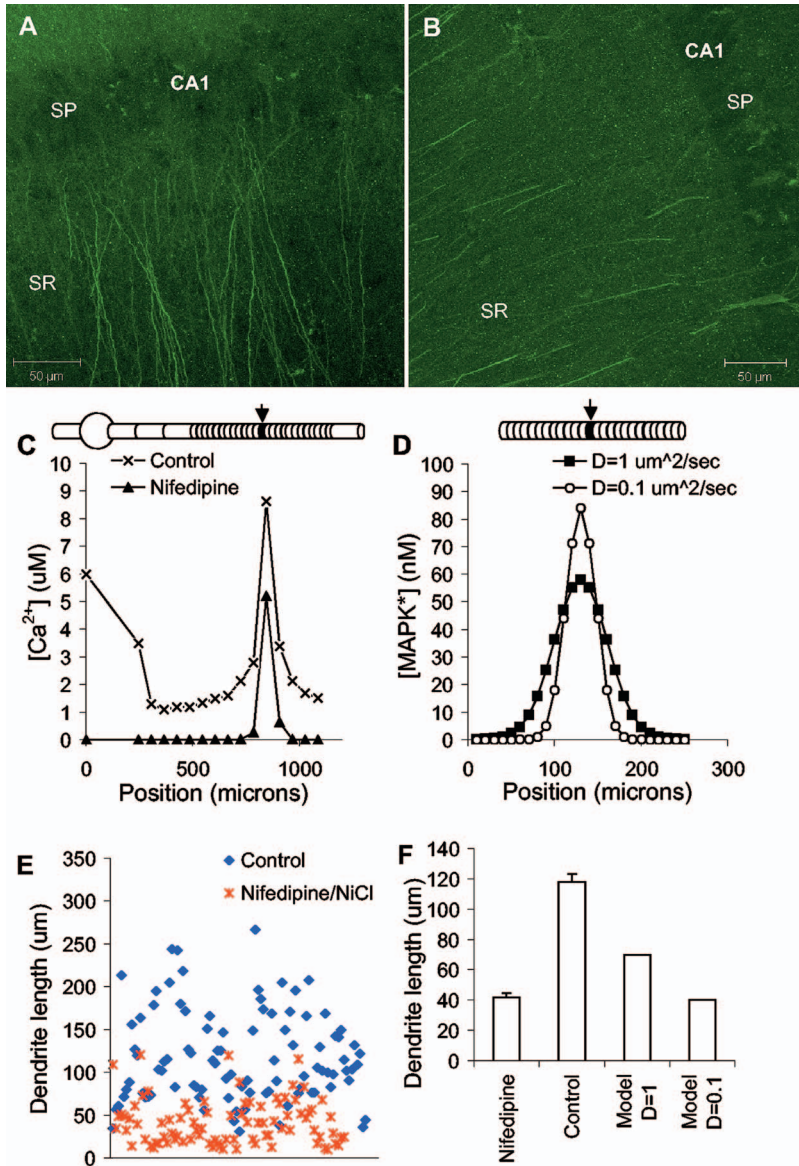


Figure 7. ERKII activation spread requires voltage-gated calcium channels (VGCCs). Confocal images of A: control slice—spaced stimuli. B: Slice treated with Nifedipine/NiCl during spaced stimuli delivery (see Methods). Dendritic staining in the treated slice is shorter than in the control. A and B: Scale bar 50 μm . C: Calcium peaks reached by the model in control and the VGCC-blocked models. The large Ca^{2+} value at position = 0 in the control case is due to somatic calcium. D: p-ERKII distribution in the model in the VGCC blocked case, for $D=1$ and $0.1 \mu m^2/s$, respectively. Input density is 50 synaptic inputs per compartment for $D=0.1 \mu m^2/s$ and 100 per compartment for $D=1 \mu m^2/s$. E: The scatter plot of lengths of activated dendrite in control and treated slices. F: Comparisons of activated dendrite length. Dendritic length for the simulations is calculated as full width at half height. Note that the $D=0.1 \mu m^2/s$ case fits the data better.

nant of ERKII activation and spread. We obtain a picture of tight ($<10 \mu m$) and strong synaptic input in small patches of the Schaffer collateral—CA1 neuron connections.

ERKII activation spread requires both diffuse input and VGCC-mediated calcium influx

At the end of this iteration through experiments and models, we had a situation where both extensive synaptic connectivity [reaction-diffusion model (4)] and dendritic Ca^{2+} influx [reaction-diffusion model (5)] appeared to be partially correct. Our interpretation is that both models are correct, but illuminate different aspects of hippocampal connectivity.

As a test of this interpretation, we modeled inputs that incorporated both the predicted broad/weak connections from the cut-slice experiment, and the punctate/strong connectivity patterns from the VGCC block experiments. We

performed several trial runs to estimate a ratio of synaptic inputs that was consistent with both sets of experiments. We found that the data were consistent when the synaptic efficacy of the broad/weak inputs was 15 times smaller than the strong/punctate inputs (Fig. 8). Because both sets of inputs were applied simultaneously, we had to reduce the strength of each input compared to the original simulations so as to obtain similar calcium peaks. We repeated the stimulus patterns for the cut-slice and VGCC experiments with these modified input strengths. The outcomes were very close to those from the above experiments and calculations in Figs. 6 and 7 [Figs. 8(A) and 8(B)]. Our estimates are restricted to the primary apical dendrite of the CA1 pyramidal neurons, but in this region they are consistent with anatomical and electrical studies of synaptic connectivity (Brivanlou *et al.*, 2004; Ishizuka *et al.*, 1990). Finally, when we simulated the

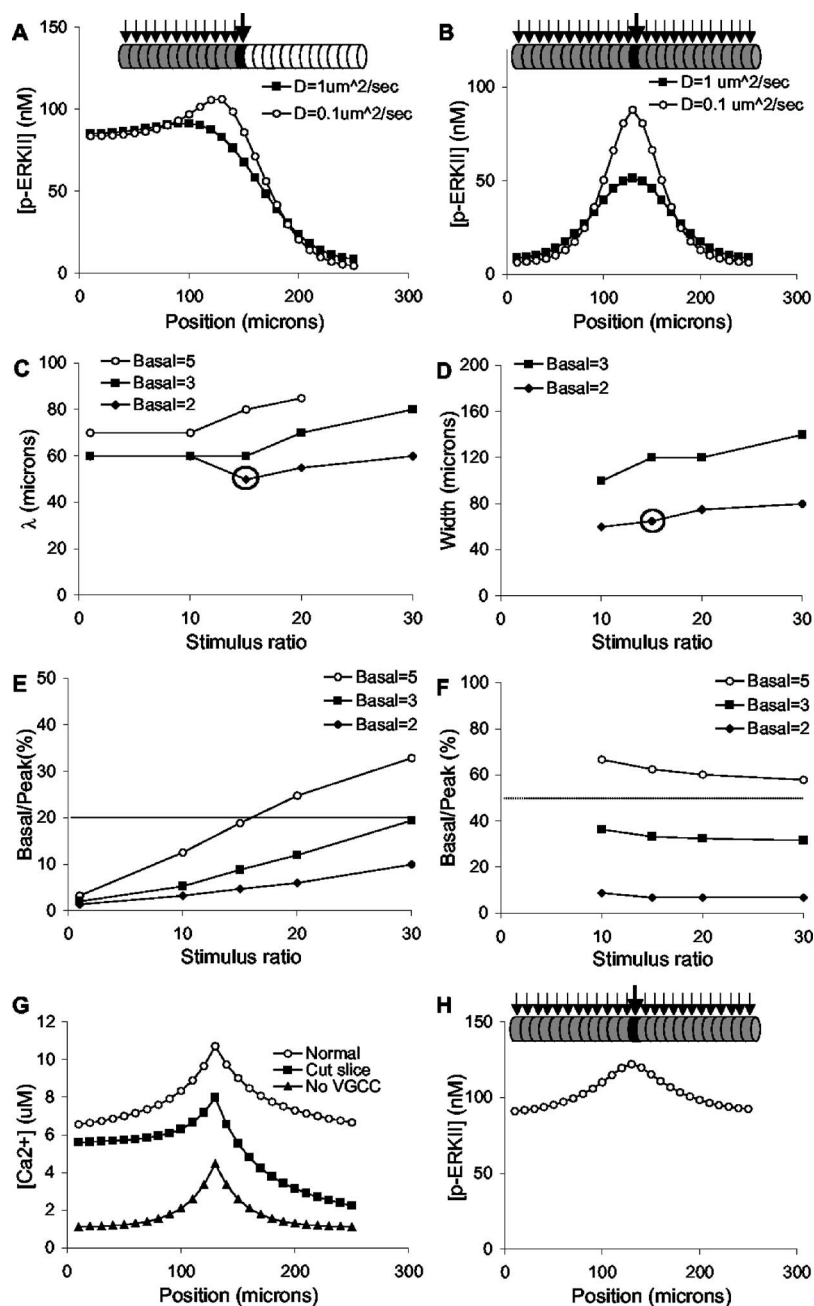


Figure 8. Combined punctate and diffuse synaptic input. A: Simulation of cut slice accounting for both contributions. Half the simulated region receives diffuse input (gray). One compartment receives strong punctate input. The remaining compartments receive no input (white). The length constant of the falloff of ERKII activation is $50 \mu\text{m}$, comparable to experiment. B: Simulation of the VGCC block accounting for both punctate and diffuse input. The entire simulation receives diffuse input (gray) with the exception of the middle compartment, which receives strong input. The peak width (full width at half height) is $60 \mu\text{m}$, comparable to experiment. C–F: Parameter exploration spanning different ratios of punctate to diffuse input and three levels of diffuse (basal) input. C: Length constant (λ) for cut-slice experiment. The selected model parameters are circled. D: The width for the VGCC block experiment. The selected model parameters are circled. E: Cut-slice experiment parameter exploration, showing the ratio of lowest response to peak response. Simulations over 20% (dashed line) were excluded. F: The parameter exploration for the VGCC block experiment showing the ratio of lowest response to peak response. Values over 50% (dashed line) were excluded. In both E and F, high basal/peak ratios are poor models because these would give extensive staining over the whole dendrite. G: Peak calcium inputs along the simulated dendrite in the normal, cut slice and VGCC block case. Note that VGCCs amplify the Ca^{2+} levels during the initial part of the stimulus (e.g., Fig. 6(E)), so the peak Ca^{2+} levels are higher than for the VGCC block case. H: The simulation of the ERKII spread with the final selected set of parameters, where both diffuse and punctate input are present and VGCC channels are active and $D=0.1 \mu\text{m}^2/\text{s}$. Extensive spread of p-ERKII activity occurs.

original experiment (with the intact slice and VGCCs), ERKII activity spread over the entire $250 \mu\text{m}$ extent of the simulated dendrite [Fig. 8(H)]. We suggest that details such as inhomogeneities in synaptic connections and dendritic tapering may contribute to the termination of ERKII spread, but these were not investigated in the current study.

In summary, we were able to understand all our experiments so far in terms of a model that included aspects of synaptic connectivity, cellular biophysics, and biochemical signaling. In this interpretation, Schaffer collateral stimulation led to the activation of many fibers that had weak connec-

tions on many neurons, and strong connections at a few points. From the viewpoint of the neuron, this translated to broad/weak input along the dendrite, along with a few strong inputs in $\sim 10 \mu\text{m}$ patches. If a neuron was sufficiently depolarized by this combination of inputs, Ca^{2+} influx occurred at stimulated synapses through NMDA receptors, and along the dendrite through VGCCs. Under our stimulus conditions, ERKII activation up to $50 \mu\text{m}$ required local Ca^{2+} input through NMDARs [Figs. 8(A) and 8(B)], and extensive spread ($>100 \mu\text{m}$) required both local input and VGCCs [Fig. 8(H)].

Extending model to *in vivo* conditions

At this point, our results had shown that extensive ERKII activation could not be explained by reaction-diffusion events alone, but also involved two distinct mechanisms for distributed Ca^{2+} influx. As the next step, we asked what the models might predict about the dynamics of spreading ERKII activation *in vivo*. In order to do this we made two important changes to the model structure. First, we provided random background synaptic activity to the electrical model to represent ongoing neuronal circuit activity in the conscious animal. Second, we integrated the electrical and biochemical models into a single functional entity by coupling the ERKII activity back into the electrical model [Fig. 9(A)]. Our model now included biophysical input to the biochemical model by way of local Ca^{2+} fluxes, and biochemical input to the biophysical model by way of local ERKII phosphorylation and inactivation of the A-type potassium (KA) channel (Frick *et al.*, 2004). All this was overlaid on the earlier loosely coupled model representations of signaling, molecular diffusion, and electrical properties of the neuron. We refer to this model as the *integrated model*. In principle we could have applied the integrated model to the earlier slice experiments, but we do not expect any difference in the model outcomes. This is because there is little background activity in the slice. In the absence of background synaptic activity, the coupling from ERKII back to the KA channel is invisible as there is no synaptic input to uncover the increased excitability of the dendrite.

Propagating ERKII activity switch

We first tested if the integrated model was formally bistable, that is, if it could switch between stable states of high or low activity. We checked ERKII activity as a function of the mean background synaptic input rate. We found that the system exhibited hysteresis in ERKII activity, which is a characteristic of bistability [Fig. 9(B)]. We also estimated thresholds for switching between high and low activity. Together with the turn-off and turn-on curves, these transition points completed the characteristic S-shaped curve of bistable systems [Fig. 9(B), open circles]. The state of low activity persisted up to a background synaptic frequency of 0.54 Hz. The state of high activity persisted down to a frequency of 0.174 Hz. In this range the system was bistable. The absolute values of these firing rates were somewhat loosely constrained in our model as we had a much-reduced model of the hippocampal neuron and approximate estimates of synaptic weights. However, the threefold range of firing over which bistability persists is a stronger prediction. For comparison, hippocampal CA3 neuron firing rates have been reported in the 0.1–0.5 Hz range in anesthetized animals (Deshmukh and Bhalla, 2003) but are around twice as high in awake recordings (e.g., Csicsvari *et al.*, 2000; Henze *et al.*, 2002).

We then examined the temporal and spatial dynamics of state switching in this system. We asked how the integrated

model responded to localized input synaptic activity riding on top of steady random background activity. We first stimulated the apical half of the neuron with a single burst of synaptic input lasting 20 s. Synaptic input ranged from 10 to 50 Hz in different test runs. With a strong stimulus (large synaptic current or high stimulus frequency) the neuron switched into an activated state. Once activated, the simulated dendrite remained in a state of heightened activity by several measures. These included frequency and amplitude of dendritic action potentials, average and peak Ca^{2+} levels in the dendrite, and activity of ERKII and PKC/PKM [Figs. 9(C) and 9(D)]. Thus, by several measures, the response of the integrated model was switch-like, and consistent with bistability. In other words, it could act like a short-term memory.

We then analyzed spatial effects. We found that we could either get propagation of activation through the entire cell, or a local and transient activation of a subset of the dendrite [Figs. 9(E) and 9(G), movies S4 and S6]. This propagation involved the mutually reinforcing activation of ERKII, leading to enhanced dendritic excitability and calcium influx [Figs. 9(A), 9(C), and 9(D)]. As expected, the outcome of a given stimulus depended both on the input strength and on the background activity. If background activity was strong and the input was strong, we were able to activate the entire 250 μm stretch of simulated dendrite with input at a single 10 μm compartment (data not shown). Small inputs did not trigger activity propagation under most conditions of background activity. Therefore, the system was quite resistant to small fluctuations in input activity.

We then tested if the active state of the dendrite could be turned off. This could be achieved by lowering background activity to below 0.1 Hz, for tens of minutes (data not shown). It could also be achieved much more rapidly by inhibitory biochemical input to the dendrite. As an example of such an input we considered inactivation/turnover of PKM. Depending both on the strength of this input, and on the background basal activity, an already active segment of dendrite could be turned back down to the state of basal activity, or the dendrite could recover back into the highly active state [Figs. 9(F) and 9(H), movies S5 and S7]. Similar to the propagation of activation along the length of the dendrite, a sufficiently strong local inhibitory input could elicit a spreading wave of inactivation that eventually would shut down the dendrite [Fig. 9(F)].

In summary, we used this final, predictive phase of our study to extrapolate our findings from the slice preparation to a more *in vivo* context with background activity. We predict that in the *in vivo* context, ERKII activation is part of a bistable, spatially extended feedback system involving A-type K^+ channel phosphorylation and an increase in dendritic excitability. Activity can trigger this switch to give both a short-term memory and also a spatially extended zone of

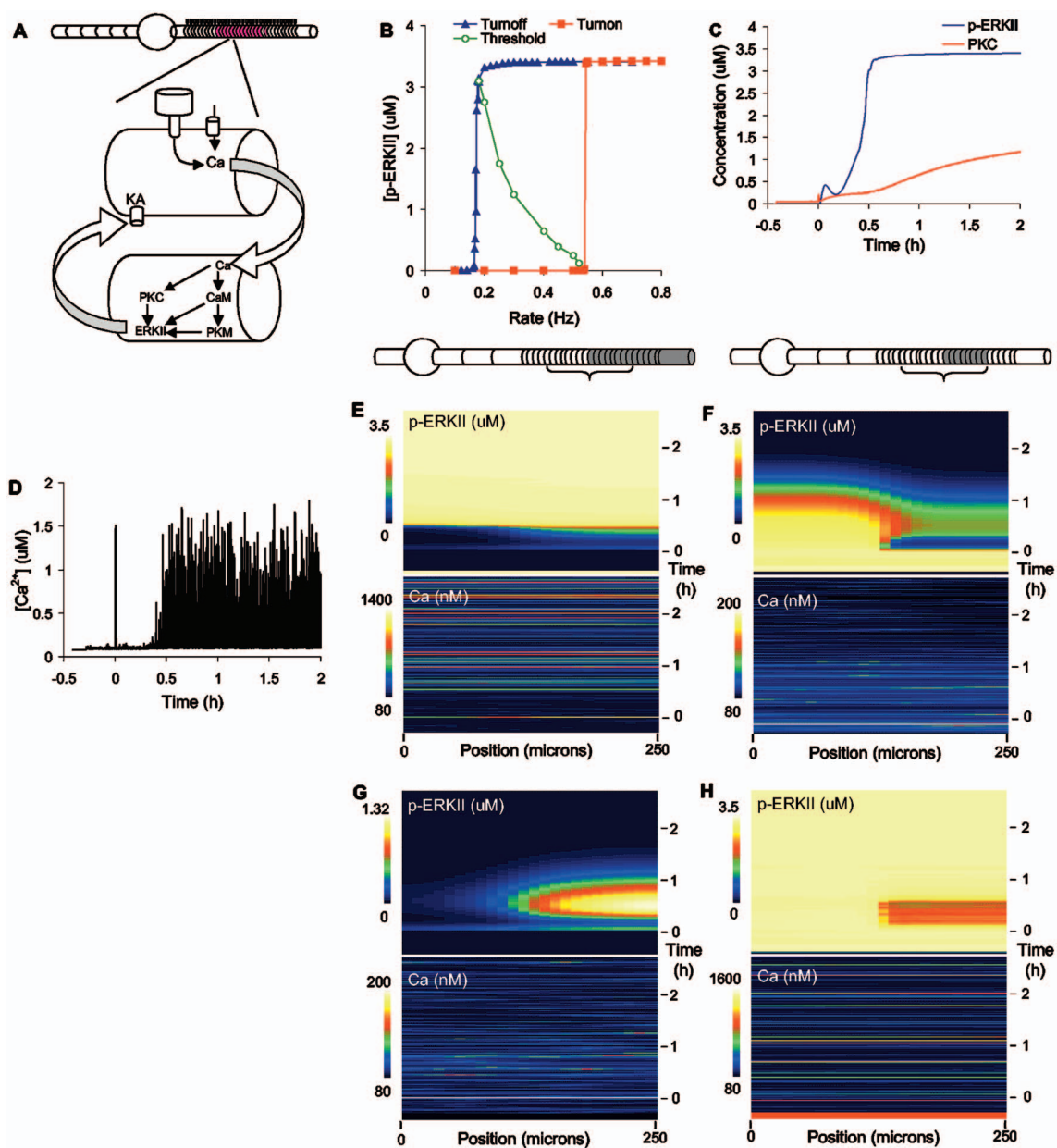


Figure 9. Propagating bistable activation in the coupled model. A: Schematic of coupling. The calcium influx into each dendritic compartment of the electrical model was coupled to the biochemical model, and acted as a stimulus. Reciprocally, the ERKII activity in the biochemical model was coupled to the KA channel in the electrical model, and reduced its conductance. This led to depolarization. B: Coupling leads to bistability over a wide range of basal synaptic input to the cell. In the range 0.18–0.5 Hz activity, the system can remain either in a state of low activity (turn-on curve) or high activity (turn-off curve), depending on activity history. The green curve is the threshold for switching. C: The time course of switching on the activity for compartment 16. The stimulus is given at $t=0$. p -ERKII builds up within half an hour. The PKC curve includes PKM activity, which builds up slowly due to synthesis. D: Ca^{2+} dynamics in compartment 16. The stimulus is a single large pulse at $t=0$. As p -ERKII builds up, the mean level of Ca^{2+} rises, due to KA inactivation that leads to dendritic action potentials. E–H: Color-coded plots of activity, with time on the vertical axis and position on the x axis. The schematic cell model shows the region of input (shaded) and the region of biochemical simulation (bracket). E: Switching on activity, from the same simulation as the curves in C and D. A burst of synaptic activity was applied for 20 s to the compartments on the right half of the electrical model. The resulting calcium and ERKII activity patterns are displayed, with position on the x axis and time increasing vertically. Within 30 min the entire 250 μm extent of the model was active. F: Switching off activity. An inhibitor of PKM was applied for 60 s to the compartments on the right half of the biochemical model. The inhibition first affects the right half of the model, then there is a partial rebound, and finally, the inhibition propagates through the entire simulated dendrite. G: The stability of the off state. A subthreshold stimulus of synaptic input was applied for 20 s to the right half of the electrical model. There is a transient local activation but it does not propagate and eventually dies away. H: Stability of the on state. PKM was partially inhibited for 1800 s in the right half of the biochemical model. After removal of the stimulus the activity of the entire dendrite recovers.

heightened electrical and biochemical activity that may influence synaptic plasticity.

DISCUSSION

In this study we showed that ERKII is activated along $>100\ \mu\text{m}$ stretches on hippocampal CA1 neurons when LTP-inducing stimuli are applied. We confirmed our hypothesis that reaction-diffusion chemistry alone could not explain this. We then tested the idea that extended Ca^{2+} input might account for the ERKII activity spread, and showed that both diffuse synaptic input and VGCC opening contribute to the spread. Finally, we predicted that feedback between biochemical and electrical events might lead to a self-sustaining switch-like propagation of ERKII activity in an *in vivo* network with sufficient background activity. This may have direct effects on L-LTP through the regulation of local synthesis of synaptic proteins, as well as influence future synaptic plasticity by altering dendritic excitability.

ERKII as a spatial signal in neurons

What role might extensive ERKII activation play in neuronal function? We suggest it is a coupling intermediate between electrical activity and neuronal signaling, especially relating to spatial interactions in synaptic plasticity (Frick and Johnston, 2005; Hausser and Mel, 2003). Our $\sim 100\ \mu\text{m}$ range of ERKII activity spread is comparable to other studies that report synaptic interactions within a $70\ \mu\text{m}$ range (Engert and Bonhoeffer, 1997). There are numerous lines of evidence for the spread of biochemical signals from synapses to dendrites on the time scale of minutes (Hama *et al.*, 2004; Schuman and Madison, 1991; Williams *et al.*, 1989). Slower homeostatic plasticity processes have recently been proposed that may also partition the dendrite into functional zones (Rabinowitch and Segev, 2006).

Three key spatial signaling processes in dendrites are synaptic tagging (Govindarajan *et al.*, 2006), heterosynaptic associativity (Sajikumar *et al.*, 2005), and activation of local protein synthesis (Blitzer *et al.*, 2005). These events share the common features of dendritic spatial scale, and a time scale of the order of minutes. Synaptic calcium influx is a likely candidate for triggering these events (Blitzer *et al.*, 2005), but specific downstream molecular targets that meet these time and space scale criteria have been difficult to identify. In the current study, the extent of ERKII activation correlates well with the length scales of such effects [$\sim 100\ \mu\text{m}$ (Engert and Bonhoeffer, 1997)], as well as the time course from a few minutes to tens of minutes. We are able to fill in many of the likely steps leading from synaptic input to ERKII activity spread over dendritic lengths. Downstream of ERKII, protein synthesis is likely to provide an input into the regulation of protein synthesis through the S6 kinase (Blitzer *et al.*, 2005; Kelleher *et al.*, 2004; Klann and Dever, 2004). We speculate that this may contribute to all three observations: tagging, heterosynaptic associativity, and of course the

local protein synthesis. Furthermore, ERKII activation is known to increase local dendritic excitability, likely through phosphorylation of an *A*-type K^+ channel (Frick *et al.*, 2004; Bernard *et al.*, 2004; Watanabe *et al.*, 2002). Our results suggest a possible mechanism by which input activity may result in such changes in dendritic excitability, and also highlight how synaptic scale activity and dendrite wide changes can be reconciled.

Model (in)completeness

Our study illustrates one of the core issues with modeling, that of deciding what to include. The most interesting systems properties in our study emerged when we integrated two distinct kinds of models, electrical and biochemical, along with spatial information. We do not suggest that important systems properties emerge only with greater model complexity. Rather, we have made a tradeoff in this study between complexity of components and the ability to model across multiple scales of cellular events. We considerably simplified our initial biochemical and biophysical models. These simplifications undoubtedly compromise the accuracy of our predictions. For example, the simulated level of ERKII activation 1 min after the stimulus in the models is not as high as the experiments suggest [Figs. 4(G)–4(I)]. Nevertheless, these approximations made our multiscale calculations tractable and lessened the number of free parameters. We suggest that there may be many biologically relevant properties that emerge not simply from complexity, but also from integrating cellular processes across multiple levels.

Switch-like changes in synaptic plasticity and dendritic excitability

One of the longstanding issues in synaptic plasticity is whether synaptic changes are analog or digital (Petersen *et al.*, 1998). An analog synapse would require a way to stably retain a given number of receptors, and possibly to control their state of phosphorylation and assembly as well. A digital synapse is easier to understand mechanistically, as it only needs two states of activity. There are several proposals for bistable switches at the synapse, involving CaMKII (Lisman and Zhabotinsky, 2001; Miller *et al.*, 2005), ERKII (Bhalla and Iyengar, 1999; Kuroda *et al.*, 2001), AMPA receptor cycling (Hayer and Bhalla, 2005), and PKA/CREB (Song *et al.*, 2006), respectively.

Our study takes the analog/digital question to the dendrite, and shows that both may coexist. We find that there is an all-or-none activation of ERKII in individual dendrites, but an effective analog readout appears because the number of such activated dendrites scales according to the stimulus pattern (Fig. 1). There are a few indications of such dendritic-level switching effects in the literature. A combined experimental and modeling study has suggested that potassium channel modulation may account for an observed

dichotomy in dendritic excitability in recordings from CA1 pyramidal neuron dendrites (Golding *et al.*, 2001). This might be indirect support for our model, which also suggests that a fraction of dendrites may be more excitable. Interestingly, there may also be alternate mechanisms for activity-dependent enhancement of CA1 excitability involving voltage-gated sodium channels, which could also contribute to switch-like activation of dendrites (Xu *et al.*, 2005).

Network implications of ERKII activity spread

Although our study is conducted at the dendritic level, there are two network-level implications that emerge from it. First, we can infer some features of network connectivity from comparing ERKII activation spread when inputs are spatially restricted, and when only synaptic sources of Ca^{2+} are available to trigger ERKII activation (Figs. 6 and 7). Our readings are consistent with a distribution of synaptic input that includes both diffuse and punctate synaptic connections onto a dendrite, from fiber bundles stimulated by an electrode. The punctate inputs appear to be restricted to 10 μm patches, and from the simulations we estimate that they are about 15 times stronger than the diffuse inputs. These punctuate, strong inputs could be clusters of synapses. Other modeling studies that have specifically explored synapse clustering and spatial distribution of synapses also indicate that the connectivity profile may have functional consequences on neuronal excitability (Azouz, 2005). From anatomical studies the hippocampal network has been characterized as sparsely connected, and on theoretical grounds such an organization may improve memory capacity (Schultz and Rolls, 1999). Our indirect estimates of functional connectivity enrich the picture of sparse strong connections with a background of diffuse connections that may be available for subsequent strengthening.

Second, our study connects network-level activity patterns to the specification of zones of dendritic excitability marked by ERKII activation. Such zonation is of interest in network studies of hippocampal function (Schultz and Rolls, 1999). We predict that the ERKII activity spread is accompanied by greater Ca^{2+} influx. This results in a feedback between biochemical and biophysical excitation in the dendrite. We speculate that it may act as a short-term switch that is active in $>100 \mu\text{m}$ zones of the dendrite. This switch is analogous to the idea of reverberating activity in neuronal circuits. Reverberating network activity is one of the oldest proposed mechanisms for short-term memory (Ermentrout and Kleinfeld, 2001; Hebb, 1949; Lorente de No, 1938; Sanchez-Vives and McCormick, 2000). In such models, electrical activity or calcium wave fronts propagate around a loop of neurons in a self-sustaining manner to store information (Loewenstein and Sompolinsky, 2003; Sidiropoulou *et al.*, 2006). Our integrated model is a dendrite-level memory that relies on background network activity, and amplifies this using reverberations between electrical and biochemical signals within the dendrite.

A further layer of network control over the cell arises because the background network input to each cell sets a threshold for activation and inactivation of this reverberation. Overall, our static images of the ERKII activation spread may be snapshots of dynamic zones of heightened excitability on the dendrite. The spatiotemporal details of network activity may interact with the propagation properties of activity in the dendrite to set up these dynamic domains primed to consolidate plasticity. Thus, the network can “paint” short-term zones onto the dendrite, in which long-term plasticity is facilitated.

EXPERIMENTAL PROCEDURES AND METHODS

Electrophysiology

450 μm transverse hippocampal slices were prepared from 4 to 6 week old male Wistar rats using a vibratory microtome (Vibratome 1000 classic series, Vibratome, USA) in ice-cold artificial cerebro-spinal fluid (*a*CSF) containing (in mM)—124 NaCl, 5 KCl, 2.5 CaCl_2 , 1.25 MgSO_4 , 1.25 NaH_2PO_4 , 26 NaHCO_3 , and 10 glucose, saturated with 95% O_2 /5% CO_2 . Slices were equilibrated in *a*CSF at room temperature for 90 min. *I/O* curves were made and baseline recordings at 40% maximum stimulus intensity that saturated the output *f*EPSP were made for 20 min. LTP was induced by using a 3×1 s high frequency stimulus (100 Hz) pattern with Inter Tetanic Interval (ITI) of 20 s (massed tetanic stimuli) or 300 s (spaced tetanic stimuli). Recordings were made for 10 min after the last tetanic stimuli in the case when slices were harvested for antibody staining or 45 min for analysis of the LTP profile. In the case of experiments performed for analyzing the time course of the spread of activated ERKII, slices were harvested at 1, 10, or 45 min after spaced tetanic stimuli. In the case of drug administration, the perfusion was switched to *a*CSF containing NiCl_2 (100 μM) and Nifedipine (10 μM) during the period of tetanic stimuli delivery. Although high levels of NiCl_2 are known to also affect the NMDA channel (Mayer and Westbrook, 1987) this effect occurs at a 200-fold higher concentration of Ni^{2+} (20 mM) than the levels we use (100 μM). Other experimental studies have used the same concentration range as we do (25–100 μM of NiCl_2) for specifically blocking voltage gated Ca^{2+} channels (*R* and *T* types) (Christie *et al.*, 1995; Hoogland and Saggau, 2004; Ito *et al.*, 1995; Magee and Johnston, 1995).

Immunohistochemistry

Ten Minutes after the last tetanic stimulus, slices were fixed at 4 °C in 4% paraformaldehyde/0.1% glutaraldehyde in PBS, pH 7.4. Slices were fixed for a period of 12–16 h. Slices were then washed for 2–3 h at room temperature in PBS. This was followed by resectioning the 400 μm slices to 40 μm slices using a vibratory microtome. Sections were rinsed in PBS-0.3% Triton X-100 (PBS-TX) (10 min), 0.75% H_2O_2 in PBS-TX (15 min) and PBS-TX (10 min \times 3). Sections were blocked with 10% normal goat serum in

PBS-TX (PBS-TX-NGS) for 1 h and incubated 12–16 h at 4 °C with primary antibodies—phospho-ERK1/II (Cell Signaling Technology, Inc., Beverly, MA) and/or microtubule associated protein 2 (MAP-2) (Sigma, Sigma-Aldrich, Inc.), total ERK I/II (Cell Signaling Technology, Inc., Beverly, MA) and phospho-CaMK II (Upstate, USA) in PBS-TX at 1:100, except *p*-CaMKII, which was used at 1:40. Sections were washed with PBS-TX (3 × 20 min each) and incubated for 2 h at room temperature with Alexa Fluor 488 goat anti-rabbit IgG (Molecular Probes, The Netherlands) and/or Alexa Fluor 563 antimouse IgG at a concentration of 1:400. Sections were washed (3 × 20 min each) and mounted on slides in 2.5% DABCO in 50% glycerol. The phospho-ERK I/II antibody recognizes both 42 KDa and 44 KDa ERK proteins, but previous studies have shown that ERK1 or 44 KDa ERK does not have a role in hippocampal LTP (Selcher *et al.*, 2001). Therefore, the results observed here were interpreted as changes in phospho-ERK II. P-ERKII staining of slices was also performed for other control conditions such as—test stimulus delivery, post AP-5 perfusion during spaced stimuli delivery and nonspecific antibody control (Supplementary Fig. S1).

Imaging and analysis

Slides prepared as mentioned above were examined at 10×, 20×, and 40× magnifications on the Olympus BX61 with fluorescence attachment. Images were captured at autoexposure times on the cooled CCD camera (Optronics). Confocal imaging was done on Zeiss LSM 510 Meta upright confocal systems with 10×, 20×, and 40× (oil) objectives. Images were acquired and analyzed on the Zeiss LSM Image browser. For all analysis, only the CA1 region between the recording and stimulating electrodes was considered. Further, after resectioning, the top 100 and bottom 100 μm of the slice were discarded and only the 200 μm were used for analysis (see the text of Fig. 1 and Supplementary Fig. S2). Statistical significance was calculated by Student’s paired *t*-test, *p* < 0.05.

Model construction

We developed our model in three stages. In the first stage we developed biochemical reaction-diffusion models, and used square calcium pulses as inputs, and *p*-ERKII levels as readouts. These models were based on a wide sample of biochemical measurements from the literature and also on our own experimental measurements in previous studies. In the

Table I. Models employed in this study (for supplementary material see EPAPS reference).

Model name	Type of model	Number of compartments	Description	Derivation
Bistable model	Biochemical	1	Feedback activation of ERKII	Ajay and Bhalla (2004)
PKM model	Biochemical	1	Feedforward activation of ERKII, PKM synthesis.	Ajay and Bhalla (2004)
Reaction-diffusion model (1)	Biochemical	25	Reaction-diffusion model	PKM model
Reaction-diffusion model (2)	Biochemical	40	Reaction-diffusion + transport model	PKM model
Reaction-diffusion model (3)	Biochemical	25	Reaction-diffusion model	Bistable model
Reaction-diffusion model (4)	Biochemical	25	Reaction-diffusion model	PKM model, identical to model (1) except for stimulus
Reaction-diffusion model (5)	Biochemical	25	Reaction-diffusion model	PKM model, identical to model (1) except for stimulus
Electrical model	Biophysical	299	Biophysical compartmental model including Ca ²⁺ dynamics	Traub (1991)
Loosely coupled model	Biophysical + biochemical	299/25	Electrical model gives Ca ²⁺ dynamics, which feed into the biochemical model	Electrical model + model (1)
Integrated model	Biophysical+ biochemical	299/25	Electrical and biochemical models feed back into each other	Loosely coupled model

second stage we also implemented a compartmental electrical model of the cell incorporating cable theory, channel biophysics, and calcium diffusion. The calcium levels generated by the electrical model were fed into the selected biochemical model from the first stage. In the third stage we elaborated the second-stage model by including biochemical feedback onto the electrical model in the form of ERKII inactivation of the KA channel. We summarize all these models in Table I. We describe the stagewise construction of all the models in the [supplementary material \(S3\)](#). The complete signaling models are available in the DOQCS database (<http://doqcs.ncbs.res.in> accession numbers 79 to 84) and all parameters are defined in [supplementary material S8](#). Some of the parameter searches for the models are shown in [supplementary material S9](#).

ACKNOWLEDGEMENTS

We thank A. Sarin, S. Chattarji at NCBS, and Temasek Life-sciences Laboratory, Singapore, for use of equipment. We thank A. Hayer, P. Rajasethupathy, A. Suvrathan and S. Deshmukh for comments. SMA and USB received support from NCBS and the DBT. USB is supported by a DAE-SRC award. SMA was supported by TIFR Alumni Endowment Fund.

Author contribution

SMA performed the experiments. USB performed the simulations. Both SMA and USB worked on the data analysis and writing.

REFERENCES

- Adams, JP, and Sweatt, JD (2002). "Molecular psychology: roles for the ERK MAP kinase cascade in memory." *Annu. Rev. Pharmacol. Toxicol.* **42**, 135–163.
- Ajay, SM, and Bhalla, US (2004). "A role for ERKII in synaptic pattern selectivity on the time-scale of minutes." *Eur. J. Neurosci.* **20**, 2671–2680.
- Azouz, R (2005). "Dynamic spatiotemporal synaptic integration in cortical neurons: neuronal gain, revisited." *J. Neurophysiol.* **94**, 2785–2796.
- Bading, H, and Greenberg, ME (1991). "Stimulation of protein tyrosine phosphorylation by NMDA receptor activation." *Science* **253**, 912–914.
- Belanger, BA, Davidian, M, and Giltinan, DM (1996). "The effect of variance function estimation on nonlinear calibration inference in immunoassay data." *Biometrics* **52**, 158–175.
- Bernard, C, Anderson, A, Becker, A, Poolos, NP, Beck, H, and Johnston, D (2004). "Acquired dendritic channelopathy in temporal lobe epilepsy." *Science* **305**, 532–535.
- Bernard, C, and Johnston, D (2003). "Distance-dependent modifiable threshold for action potential back-propagation in hippocampal dendrites." *J. Neurophysiol.* **90**, 1807–1816.
- Bhalla, US, and Iyengar, R (1999). "Emergent properties of networks of biological signaling pathways." *Science* **283**, 381–387.
- Bhalla, US, Ram, PT, and Iyengar, R (2002). "MAP kinase phosphatase as a locus of flexibility in a mitogen-activated protein kinase signaling network." *Science* **297**, 1018–1023.
- Blitzer, RD, Iyengar, R, and Landau, EM (2005). "Postsynaptic signaling networks: cellular cogwheels underlying long-term plasticity." *Biol. Psychiatry* **57**, 113–119.
- Bower, JM, and Beeman, D (1998). *The Book of GENESIS*, Springer, Santa Clara.
- Brivanlou, IH, Dantzer, JL, Stevens, CF, and Callaway, EM (2004). "Topographic specificity of functional connections from hippocampal CA3 to CA1." *Proc. Natl. Acad. Sci. U.S.A.* **101**, 2560–2565.
- Christie, BR, Eliot, LS, Ito, K, Miyakawa, H, and Johnston, D (1995). "Different Ca²⁺ channels in soma and dendrites of hippocampal pyramidal neurons mediate spike-induced Ca²⁺ influx." *J. Neurophysiol.* **73**, 2553–2557.
- Csicsvari, J, Hirase, H, Mamiya, A, and Buzsaki, G (2000). "Ensemble patterns of hippocampal CA3-CA1 neurons during sharp wave-associated population events." *Neuron* **28**, 585–594.
- Deshmukh, SS, and Bhalla, US (2003). "Representation of odor habituation and timing in the hippocampus." *J. Neurosci.* **23**, 1903–1915.
- Dudek, SM, and Fields, RD (2001). "Mitogen-activated protein kinase/extracellular signal-regulated kinase activation in somatodendritic compartments: roles of action potentials, frequency, and mode of calcium entry." *J. Neurosci.* **21**, RC122.
- Engert, F, and Bonhoeffer, T (1997). "Synapse specificity of long-term potentiation breaks down at short distances." *Nature (London)* **388**, 279–284.
- EPAPS document No. E-HJFOA5-1-004701 for supplemental material. This document can be reached through a direct link in the online article's HTML reference section or via the EPAPS homepage (<http://www.aip.org/pubservs/epaps.html>).
- Ermentrout, GB, and Kleinfeld, D (2001). "Traveling electrical waves in cortex: insights from phase dynamics and speculation on a computational role." *Neuron* **29**, 33–44.
- Frey, U, and Morris, RG (1997). "Synaptic tagging and long-term potentiation." *Nature (London)* **385**, 533–536.
- Frick, A, and Johnston, D (2005). "Plasticity of dendritic excitability." *J. Neurophysiol.* **64**, 100–115.
- Frick, A, Magee, J, and Johnston, D (2004). "LTP is accompanied by an enhanced local excitability of pyramidal neuron dendrites." *Nat. Neurosci.* **7**, 126–135.
- Golding, NL, Kath, WL, and Spruston, N (2001). "Dichotomy of action-potential backpropagation in CA1 pyramidal neuron dendrites." *J. Neurophysiol.* **86**, 2998–3010.
- Govindarajan, A, Kelleher, RJ, and Tonegawa, S (2006). "A clustered plasticity model of long-term memory engrams." *Nat. Rev. Neurosci.* **7**, 575–583.
- Hama, H, Hara, C, Yamaguchi, K, and Miyawaki, A (2004). "PKC signaling mediates global enhancement of excitatory synaptogenesis in neurons triggered by local contact with astrocytes." *Neuron* **41**, 405–415.
- Hausser, M, and Mel, B (2003). "Dendrites: bug or feature?" *Curr. Opin. Neurobiol.* **13**, 372–383.
- Hausser, M, Spruston, N, and Stuart, GJ (2000). "Diversity and dynamics of dendritic signaling." *Science* **290**, 739–744.
- Hayer, A, and Bhalla, US (2005). "Molecular switches at the synapse emerge from receptor and kinase traffic." *PLOS Comput. Biol.* **1**, 137–154.
- Hebb, DO (1949). *The Organization of Behavior*, Wiley, New York.
- Henze, DA, Wittner, L, and Buzsaki, G (2002). "Single granule cells reliably discharge targets in the hippocampal CA3 network in vivo." *Nat. Neurosci.* **5**, 790–795.
- Hernandez, AI, Blace, N, Crary, JF, Serrano, PA, Leitges, M, Libien, JM, Weinstein, G, Tcherapanov, A, and Sacktor, TC (2003). "Protein kinase M zeta synthesis from a brain mRNA encoding an independent protein kinase C zeta catalytic domain. Implications for the molecular mechanism of memory." *J. Biol. Chem.* **278**, 40305–40316.
- Hoogland, TM, and Saggau, P (2004). "Facilitation of L-type Ca²⁺ channels in dendritic spines by activation of beta2 adrenergic receptors." *J. Neurosci.* **24**, 8416–8427.
- Ishizuka, N, Weber, J, and Amaral, DG (1990). "Organization of intrahippocampal projections originating from CA3 pyramidal cells in the rat." *J. Comp. Neurol.* **295**, 580–623.
- Ito, K, Miura, M, Furuse, H, Zhixiong, C, Kato, H, Yasutomi, D, Inoue, T, Mikoshiba, K, Kimura, T, Sakakibara, S, et al. (1995). "Voltage-gated Ca²⁺ channel blockers, omega-AgaIVA and Ni²⁺, suppress the induction of theta-burst induced long-term potentiation in guinea-pig hippocampal CA1 neurons." *Neurosci. Lett.* **183**, 112–115.
- Kelleher, RJ, 3rd, Govindarajan, A, Jung, HY, Kang, H, and Tonegawa, S (2004). "Translational control by MAPK signaling in long-term

- synaptic plasticity and memory." *Cell* **116**, 467–479.
- Kennedy, MJ, and Ehlers, MD (2006). "Organelles and trafficking machinery for postsynaptic plasticity." *Annu. Rev. Neurosci.* **29**, 325–362.
- Kholodenko, BN (2003). "Four-dimensional organization of protein kinase signaling cascades: the roles of diffusion, endocytosis and molecular motors." *J. Exp. Biol.* **206**, 2073–2082.
- Klann, E, and Dever, TE (2004). "Biochemical mechanisms for translational regulation in synaptic plasticity." *Nat. Rev. Neurosci.* **5**, 931–942.
- Kuroda, S, Schweighofer, N, and Kawato, M (2001). "Exploration of signal transduction pathways in cerebellar long-term depression by kinetic simulation." *J. Neurosci.* **21**, 5693–5702.
- Lisman, JE, and Zhabotinsky, AM (2001). "A model of synaptic memory: a CaMKII/PP1 switch that potentiates transmission by organizing an AMPA receptor anchoring assembly." *Neuron* **31**, 191–201.
- Loewenstein, Y, and Sompolinsky, H (2003). "Temporal integration by calcium dynamics in a model neuron." *Nat. Neurosci.* **6**, 961–967.
- Lorente de No, R (1938). "Analysis of the activity of the chains of internuncial neurons." *J. Neurophysiol.* **1**, 207–244.
- Magee, JC, and Johnston, D (1995). "Synaptic activation of voltage-gated channels in the dendrites of hippocampal pyramidal neurons." *Science* **268**, 301–304.
- Mayer, ML, and Westbrook, GL (1987). "Permeation and block of *N*-methyl-D-aspartic acid receptor channels by divalent cations in mouse cultured central neurones." *J. Physiol.* **394**, 501–527.
- Miller, P, Zhabotinsky, AM, Lisman, JE, and Wang, XJ (2005). "The stability of a stochastic CaMKII switch: dependence on the number of enzyme molecules and protein turnover." *PLoS Biol.* **3**, e107.
- Morozov, A, Muzzio, IA, Bourchouladze, R, Van-Strien, N, Lapidus, K, Yin, D, Winder, DG, Adams, JP, Sweatt, JD, and Kandel, ER (2003). "Rap1 couples cAMP signaling to a distinct pool of p42/44MAPK regulating excitability, synaptic plasticity, learning, and memory." *Neuron* **39**, 309–325.
- Petersen, CC, Malenka, RC, Nicoll, RA, and Hopfield, JJ (1998). "All-or-none potentiation at CA3-CA1 synapses." *Proc. Natl. Acad. Sci. U.S.A.* **95**, 4732–4737.
- Rabinowitch, I, and Segev, I (2006). "The endurance and selectivity of spatial patterns of long-term potentiation/depression in dendrites under homeostatic synaptic plasticity." *J. Neurosci.* **26**, 13474–13484.
- Reeves, GT, Muratov, CB, Schupbach, T, and Shvartsman, SY (2006). "Quantitative models of developmental pattern formation." *Dev. Cell* **11**, 289–300.
- Reynolds, AR, Tischer, C., Verveer, PJ, Rocks, O, and Bastiaens, PI (2003). "EGFR activation coupled to inhibition of tyrosine phosphatases causes lateral signal propagation." *Nat. Cell Biol.* **5**, 447–453.
- Roberson, ED, English, JD, Adams, JP, Selcher, JC, Kondratieck, C, and Sweatt, JD (1999). "The mitogen-activated protein kinase cascade couples PKA and PKC to cAMP response element binding protein phosphorylation in area CA1 of hippocampus." *J. Neurosci.* **19**, 4337–4348.
- Rudolph, M, and Destexhe, A (2003). "A fast-conducting, stochastic integrative mode for neocortical neurons in vivo." *J. Neurosci.* **23**, 2466–2476.
- Sajikumar, S, Navakkode, S, Sacktor, TC, and Frey, JU (2005). "Synaptic tagging and cross-tagging: the role of protein kinase Mzeta in maintaining long-term potentiation but not long-term depression." *J. Neurosci.* **25**, 5750–5756.
- Sanchez-Vives, MV, and McCormick, DA (2000). "Cellular and network mechanisms of rhythmic recurrent activity in neocortex." *Nat. Neurosci.* **3**, 1027–1034.
- Schultz, SR, and Rolls, ET (1999). "Analysis of information transmission in the Schaffer collaterals." *Hippocampus* **9**, 582–598.
- Schuman, EM, and Madison, DV (1991). "A requirement for the intercellular messenger nitric oxide in long-term potentiation." *Science* **254**, 1503–1506.
- Selcher, JC, Nekrasova, T, Paylor, R, Landreth, GE, and Sweatt, JD (2001). "Mice lacking the ERK1 isoform of MAP kinase are unimpaired in emotional learning." *Learn. Memory* **8**, 11–19.
- Sidiropoulou, K, Pissadaki, EK, and Poirazi, P (2006). "Inside the brain of a neuron." *EMBO Rep.* **7**, 886–892.
- Song, H, Smolen, P, Av-Ron, E, Baxter, DA, and Byrne, JH (2006). "Bifurcation and singularity analysis of a molecular network for the induction of long-term memory." *Biophys. J.* **90**, 2309–2325.
- Thiels, E, and Klann, E (2001). "Extracellular signal-regulated kinase, synaptic plasticity, and memory." *Rev. Neurosci.* **12**, 327–345.
- Traub, RD, Wong, RK, Miles, R, and Michelson, H (1991). "A model of a CA3 hippocampal pyramidal neuron incorporating voltage-clamp data on intrinsic conductances." *J. Neurophysiol.* **66**, 635–650.
- Urakubo, H, Aihara, T, Kuroda, S, Watanabe, M, and Kondo, S. (2004). "Spatial localization of synapses required for supralinear summation of action potentials and EPSPs." *J. Comput. Neurosci.* **16**, 251–265.
- Watanabe, S, Hoffman, DA, Migliore, M, and Johnston, D (2002). "Dendritic K⁺ channels contribute to spike-timing dependent long-term potentiation in hippocampal pyramidal neurons." *Proc. Natl. Acad. Sci. U.S.A.* **99**, 8366–8371.
- Williams, JH, Errington, ML, Lynch, MA, and Bliss, TV (1989). "Arachidonic acid induces a long-term activity-dependent enhancement of synaptic transmission in the hippocampus." *Nature (London)* **341**, 739–742.
- Wu, GY, Deisseroth, K, and Tsien, RW (2001). "Spaced stimuli stabilize MAPK pathway activation and its effects on dendritic morphology." *Nat. Neurosci.* **4**, 151–158.
- Xu, J, Kang, N, Jiang, L, Nedergaard, M, and Kang, J (2005). "Activity-dependent long-term potentiation of intrinsic excitability in hippocampal CA1 pyramidal neurons." *J. Neurosci.* **25**, 1750–1760.
- Ying, SW, Futter, M, Rosenblum, K, Webber, MJ, Hunt, SP, Bliss, TV, and Bramham, CR (2002). "Brain-derived neurotrophic factor induces long-term potentiation in intact adult hippocampus: requirement for ERK activation coupled to CREB and upregulation of arc synthesis." *J. Neurosci.* **22**, 1532–1540.
- Yuan, LL, Adams, JP, Swank, M, Sweatt, JD, and Johnston, D (2002). "Protein kinase modulation of dendritic K⁺ channels in hippocampus involves a mitogen-activated protein kinase pathway." *J. Neurosci.* **22**, 4860–4868.
- Zhu, JJ, Qin, Y, Zhao, M, Van Aelst, L, and Malinow, R (2002). "Ras and Rap control AMPA receptor trafficking during synaptic plasticity." *Cell* **110**, 443–455.